FFEMS Fatigue & Fracture of Engineering Materials & Structures

doi: 10.1111/ffe.12032

# Analysis of mechanical properties and its associated fracture surfaces in dual-phase austempered ductile iron

**A. BASSO, J. SIKORA and R. MARTÍNEZ**

*Facultad de Ingeniería – INTEMA, Universidad Nacional de Mar del Plata – CONICET, Av. Juan B. Justo 4302, B7608FDQ Mar del Plata, Argentina*

*Received in final form 3 July 2012*

**ABSTRACT** This work aims at evaluating the fracture surfaces of tensile samples taken from a new kind of ductile iron referred to as 'dual-phase Austempered Ductile Iron (ADI)', a material composed of ausferrite (regular ADI microstructure) and free (or allotriomorphic) ferrite. The tensile fracture surface characteristics and tensile properties of eight dual-phase ADI microstructures, containing different relative quantities of ferrite and ausferrite, were studied in an alloyed ductile cast iron. Additionally, samples with fully ferritic and fully ausferritic (ADI) matrices were produced to be used as reference. Ferritic–pearlitic ductile irons (DI) were evaluated as well. For dual-phase ADI microstructures, when the amount of ausferrite increases, tensile strength, yield stress and hardness do so too. Interesting combinations of strength and elongation until failure were found. The mechanisms of fracture that characterise DI under static uniaxial loading at room temperature are nucleation, growth and coalescence of microvoids. The fracture surface of fully ferritic DI exhibited an irregular topography with dimples and large deformation of the nodular cavities, characteristic of ductile fracture. Microstructures with small percentages of ausferrite (less than 20%) yielded better mechanical properties in relation to fully ferritic matrices. These microstructures presented regions of quasi-cleavage fracture around last-to-freeze zones, related to the presence of ausferrite in those areas. As the amount of ausferrite increased, a decrease in nodular cavities deformation and a flatter fracture surface topography were noticed, which were ascribed to a higher amount of quasi-cleavage zones. By means of a special thermal cycle, microstructures with pearlitic matrices containing a continuous and well-defined net of allotriomorphic ferrite, located at the grain boundaries of recrystallised austenite, were obtained. The results of the mechanical tests leading to these microstructures revealed a significant enhancement of mechanical properties with respect to completely pearlitic matrices. The topographies of the fracture surfaces revealed a flat aspect and slightly or undeformed nodular cavities, as a result of high amount of pearlite. Still isolated dimple patterns associated to ferritic regions were observed.

**Keywords** dual-phase ADI; ductile iron; fracture surfaces; matrix microstructure.

**NOMENCLATURE**

$ADI$ = Austempered Ductile Iron
$HTA$ = Heat Treatment "A"
$HTB$ = Heat Treatment "B"
$T_\gamma$ = Austenitising temperature
$\alpha$ = Ferrite
$\gamma$ = Austenite
$\delta(\%)$ = elongation until failure
$\sigma_{0.2}$ = yield stress
$\sigma_{uts}$ = ultimate tensile stress

*Correspondence:* R. Martínez, E-mail: rimarti@fi.mdp.edu.ar
This work is dedicated to the memory of Jorge Sikora.


 

## INTRODUCTION

Producers of ductile iron (DI) have focused their efforts in improving mechanical properties in the search of new applications, specifically in the market of automotive critical parts in terms of safety in which toughness and high strength are primary requirements.

In recent past years, a new type of DI has been under development: the new material called dual-phase ADI in which matrix is composed of ausferrite and free (or allotriomorphic) ferrite.

To obtain the aforementioned microstructure, different methodologies have been applied, such as changes in the chemical composition and using a thermal cycle with incomplete austenitisation laying into the intercritical interval of the Fe-C-Si diagram followed by an austempering in a salt bath.[1] Another attempt[2] was carried out using heat treatments based on quick and incomplete austenitisations, the austenite obtained at high temperature being converted in ausferrite after an austempering step.

The authors of this paper[4,5] and Kilicli *et al.*[6,7] proposed an alternative to the previous approaches, which consists of an incomplete austenitisation stage at temperatures within the intercritical interval, followed by austempering and transforming the high temperature austenite to room temperature ausferrite. The selections of different intercritical temperatures make it possible to obtain different combinations of free ferrite–ausferrite percentages.

Several studies have been devoted to determining the mechanical response, mainly the tensile properties. The results confirm that dual-phase ADI provides a wide range of mechanical properties depending on the relative fraction of the microconstituents in the matrix.

Aranzabal *et al.*[1] reported that the yield stress and tensile strength values of dual-phase ADI, together with its hardness, are similar to those of fully pearlitic DI, whereas ductility presents the same level as ferritic DI. Wade *et al.*[2] and Verdu *et al.*[3] assessed the mechanical properties of dual-phase ADI microstructures austempered at 375 °C with ferrite as the majority phase and encapsulating graphite nodules with ausferrite. They found that yield stress, tensile strength and hardness increased as the ausferrite volume fraction in the microstructure did.

Works carried out by Kilicli *et al.*[6,7] were focused on dual-phase ADI mechanical properties, particularly for those austempered at 365 °C and a wide variety of ferrite–ausferrite combinations. An interesting result was for the 45% ausferrite and 65% ferrite microstructure that yielded the best strength–toughness combination.

The authors of this paper have also investigated this topic, analysing the part that the amount and morphologies of phases, austempering temperature and cast part size play in the final microstructure and its properties.[4,5] As expected, as the amount of ausferrite increased, so did tensile strength and yield stress, whereas elongation decreased for all the austempering temperatures investigated.

The best combinations of strength and elongation corresponded to dual-phase ADI microstructures austempered at 350 °C.[4]

The promising results obtained in this preliminary work led the authors to conduct further research. The main objective of this work was to study the most significant characteristics of fracture surfaces, obtained by means of tensile tests from different samples of dual-phase ADI, centring their attention on the relationship between the observed fracture surface and the tensile properties obtained. The first paper dealing with this topic was that by Kilicli *et al.*[8] The authors reported diverse fracture mechanisms corresponding to the different levels of ausferrite volume fractions in the dual-phase ADI structures.

## EXPERIMENTAL METHODOLOGY

### Material

A ductile cast iron melt was prepared in a medium frequency induction furnace. Steel scrap and foundry returns were used as raw materials. The nodulisation step was carried out using the sandwich method and 1.5% of Fe-Si-Mg (6% mg). The melt was then inoculated with 0.6% Fe-Si (75% Si). Cu and Ni were added in order to obtain adequate austemperability. The chemical composition of the melt was determined by using a Baird (*Baird corporation*. 27 Forge Parkway. *Franklin*, *MA* 02038-3135 - USA) DV6 spectrometer. One inch 'Y' blocks were cast in sand moulds (ASTM A395). Round bars of 12 mm diameter were cut from the Y blocks and were used to produce metallographic and mechanical test samples.

### Heat treatments

All the bars were ferritised by annealing at 900 °C for 3 h using an electric furnace, followed by a slow cooling stage in order to obtain fully ferritic matrices in all the samples used in the present study.

#### *Determination of the intercritical interval*

The intercritical interval for the melt was established by employing the methodology described in previous papers by the authors,[4,5] which is herein summarised as follows: ferritised specimens were subjected to thermal cycles involving austenitising stages at temperatures ranging from 720 to 900 °C, at steps of 20 °C. Each complete thermal cycle consisted of holding the sample for 1 h in the furnace at each selected temperature ($T\gamma$). After the heating step, samples were water quenched. The resulting

microstructures were composed of different amounts of ferrite (original matrix) and martensite (quenched austenite). It is worth mentioning that, on the basis of previous works, a holding time of about 30 min is enough to reach the equilibrium phase percentages in the $\alpha \rightarrow \gamma$ transformation within the intercritical interval, starting from fully ferritic matrices. The ferritising and austenitising treatments were both performed using electric furnaces, whereas for austempering, a 500 kg salt bath was used.

### *Heat treatments to produce dual-phase ADI*

Eight dual-phase ADI microstructures, containing different relative quantities of ferrite and ausferrite, were obtained by means of high-temperature austenitization called Heat Treatment "A" (HTA), which consisted in a partial austenitisation of the samples by holding them in the furnace within the intercritical interval at 760, 770, 790, 800, 820, 830, 840 and 850 °C for 60 min, followed by an austempering step at 350 °C for 90 min in all the cases (Fig. 1). Additionally, samples with fully ferritic and fully ausferritic matrices (ADI) were produced for reference purposes. ADI samples were obtained by means of a heat treatment consisting in a complete austenitising stage at 910 C for 60 min, followed by an austempering step at 350 °C for 90 min.

The quantification of the relationship between the amount (% in volume) of ferrite and ausferrite in the dual-phase ADI microstructures was measured by using an optical microscope and the Image Pro Plus software, following experimental procedures described in the bibliography.[9] Reported values are the average of at least five determinations on each sample. Graphite areas were not considered in the percentage of the reported microconstituents.

As postulated by the authors in a previous work,[10] different variants of dual-phase ADI microstructures can be obtained depending on the heat treatment used. In this work, a second heat treatment cycle, called Heat Treatment "B" (HTB), was used to study the possibility of producing different variants of dual-phase ADI microstructures. This heat treatment is sketched in Fig. 2 and consists in a first step of a complete austenitisation by holding the samples well above the upper critical temperature (910 °C) for 60 min in an electric furnace. Afterwards, they are rapidly transferred to a salt bath at a temperature of 800 °C (temperature within the intercritical interval) and held at different times, 60, 120 and 180 min. This second stage allows for proeutectoid ferrite nucleation and favours growth on the austenitic matrix ($\gamma \rightarrow \alpha$ reaction) as a function of holding time. Then, samples are removed from the salt bath and air cooled, rather than being subjected to an austempering step. The resulting microstructures are composed of different amounts of ferrite and pearlite. This type of microstructure (ferritic–pearlitic) was selected as a preliminary study on the basis of results published by Galarreta *et al.*[11] who reported results of mechanical tests performed on a novel microstructure composed of a pearlitic matrix containing a continuous net of ferrite. The authors accounted for a significant enhancement of the mechanical properties in this kind of microstructure, with respect to completely pearlitic matrices.

### *Tensile test*

Tensile tests were conducted in agreement with the ASTM E8-M standard, using a universal testing machine (INSTRON 8501). The values of all the properties reported are the average of testing at least three samples. Fracture surfaces were analysed by scanning electron microscopy (SEM). Hardness values were determined following the procedure given by the ASTM E-10 standard.

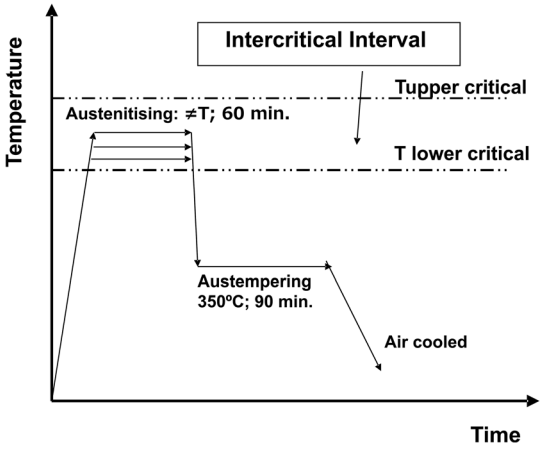


**Fig. 1** Heat treatment HTA employed to produce dual phase ADI microstructures.

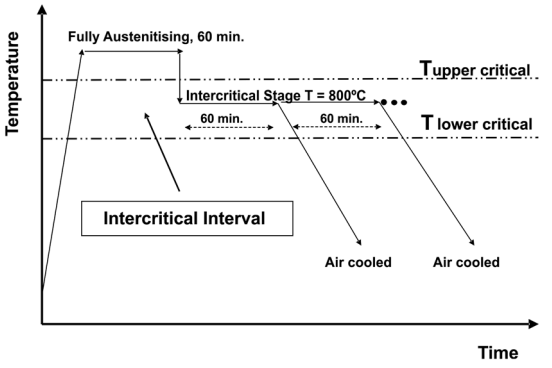


**Fig. 2** Heat treatment HTB employed to produce ferritic-pearlitic microstructures.

## RESULTS

### Microstructures and tensile properties

The melt used in this paper had a chemical composition as listed in Table 1. The as-cast microstructure offered 150 nod/mm$^2$ of size 5 with 90% nodularity, according to the ASTM A 247 standard. The as-cast microstructure of the metallic matrix was composed of 85% pearlite and 15% ferrite. The metallic matrix of all samples was fully ferritic, after the annealing heat treatment. The lower critical temperature (the temperature at the ferrite → austenite transformation start) was defined as 750 °C. The upper critical temperature was established as 870 °C, considering that a matrix with over 98% martensite was obtained in samples held at such a temperature.

The main characteristics of the samples used in this study such as dual-phase ADI microstructure, amount of phases and mechanical properties are listed in Tables 2 and 3. Also included are the same parameters for fully pearlitic and fully ferritic microstructures.

**Table 1** Chemical Composition of the Melt (%).

| C | Si | Mn | Cu | Ni | Mg | P | S | CE |
|---|---|---|---|---|---|---|---|---|
| 3.39 | 2.61 | 0.37 | 0.65 | 0.87 | 0.052 | 0.04 | 0.04 | 4.25 |

The microstructures of two dual-phase ADI samples austenitised at 790 and 820 °C are depicted in Fig. 3. They were austenitised within the intercritical interval and then austempered in a salt bath at 350 °C (samples HTA-2 and HTA-5), together with fully ferritic DI (F) and a regular ADI sample. As depicted in this figure, the HTA used to produce dual-phase ADI allowed microstructures composed of different percentages of ausferrite and allotriomorphic ferrite using different intercritical austenitisation temperatures to be obtained.

As the amount of ausferrite increases in dual-phase ADI (obtained by HTA heat treatment), tensile strength, yield stress and hardness also increase. Some combinations of strength and elongation found deserve special attention such as the microstructure composed of 20% ferrite and 80% ausferrite, which combines a tensile strength of 800 MPa with an elongation until failure of 23%. These results are in agreement with values reported by other authors in the bibliography.[1–8] For the ferritic–pearlitic DI, obtained using HTB, a microstructure composed of a pearlitic matrix containing a continuous net of

**Table 2** Sample designation, parameters of the heat treatment, microconstituents percentages and mechanical properties for Dual Phase ADI employing HTA.

| Sample | Heat treatment employed | Austenitising and austempering temperatures (°C) | Ausferrite volume fraction | Ferrite volume fraction | $\sigma_{uts}$ (MPa) | $\sigma_{0.2}$ (MPa) | δ (%) | Hardness (Brinell) |
|---|---|---|---|---|---|---|---|---|
| F | As annealing | – | ≈0 | ≈100 | 521 | 360 | 25 | 163 |
| HTA-1 | HTA | 760, 350 | ≈10 | ≈90 | 529 | 385 | 24 | 165 |
| HTA-2 | HTA | 770, 350 | ≈15 | ≈85 | 533 | 404 | 25 | 177 |
| HTA-3 | HTA | 790, 350 | ≈40 | ≈60 | 587 | 442 | 23 | 195 |
| HTA-4 | HTA | 800, 350 | ≈60 | ≈40 | 715 | 486 | 22 | 214 |
| HTA-5 | HTA | 820, 350 | ≈80 | ≈20 | 800 | 632 | 23 | 246 |
| HTA-6 | HTA | 840, 350 | ≈85 | ≈15 | 821 | 651 | 20 | 260 |
| HTA-7 | HTA | 850, 350 | ≈90 | ≈10 | 845 | 699 | 19 | 262 |
| HTA-8 | HTA | 860, 350 | ≈95 | ≈5 | 987 | 846 | 16 | 292 |
| ADI | Conventional austempering | 910, 350 | 100 | 0 | 1108 | 929 | 10 | 321 |

*Graphite areas were not considered in the percentage of the reported microconstituents.

**Table 3** Sample designation, parameters of the heat treatment, microconstituents percentages and mechanical properties for ferritic-pearlitic DI employing HTB.

| Sample | Heat treatment employed | Intercritical temperature and time | Pearlite volume fraction | Ferrite volume fraction | $\sigma_{uts}$ (MPa) | $\sigma_{0.2}$ (MPa) | δ (%) | Hardness (Brinell) |
|---|---|---|---|---|---|---|---|---|
| HTB-1 | HTB | 800 °C, 60 min | ≈85 | ≈5 | 1050 | 600 | 6 | 317 |
| HTB-2 | HTB | 800 °C, 120 min | ≈90 | ≈10 | 1000 | 550 | 6 | 310 |
| HTB-3 | HTB | 800 °C, 180 min | ≈95 | ≈15 | 990 | 500 | 7 | 289 |
| P | Conventional normalised | Air cooled from austenitising temperature | 100 | 0 | 1120 | 800 | 4 | 325 |

*Graphite areas were not considered in the percentage of the reported microconstituents.

ferrite located at the grain boundaries of recrystallised austenite was obtained, just as described by Galarreta *et al.*[11] The microstructures composed of ferrite precipitated at the grain boundaries of the recrystallised austenite produced after the complete austenitisation step, during the intercritical stage, are shown in Fig. 4, with 5, 10 and 15% of ferrite for HTB1, HTB2, and HTB3, respectively.

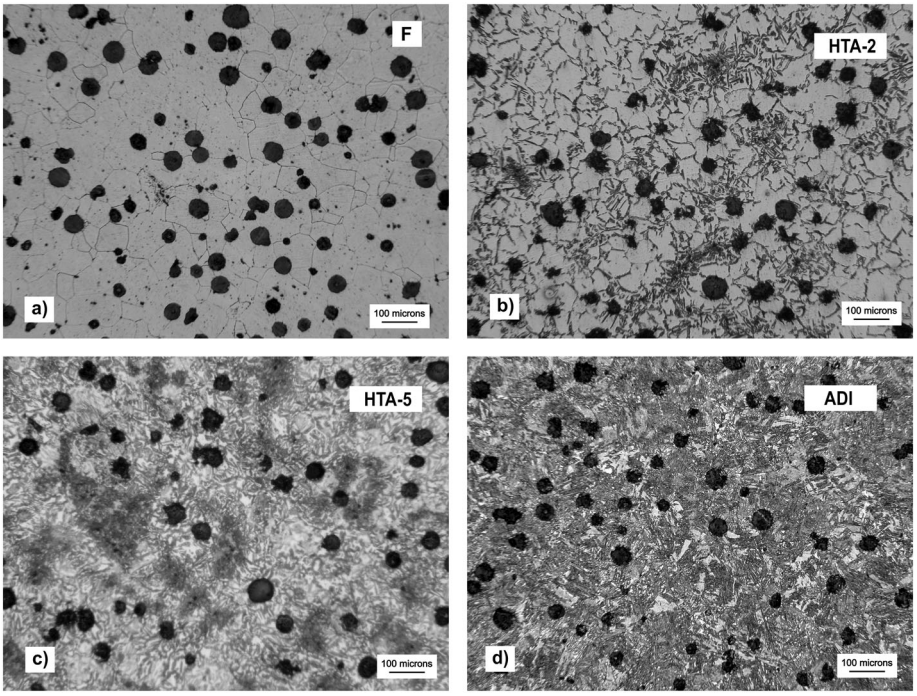


**Fig. 3** Micrographs of F, HTA-2, HTA-5, and ADI samples.

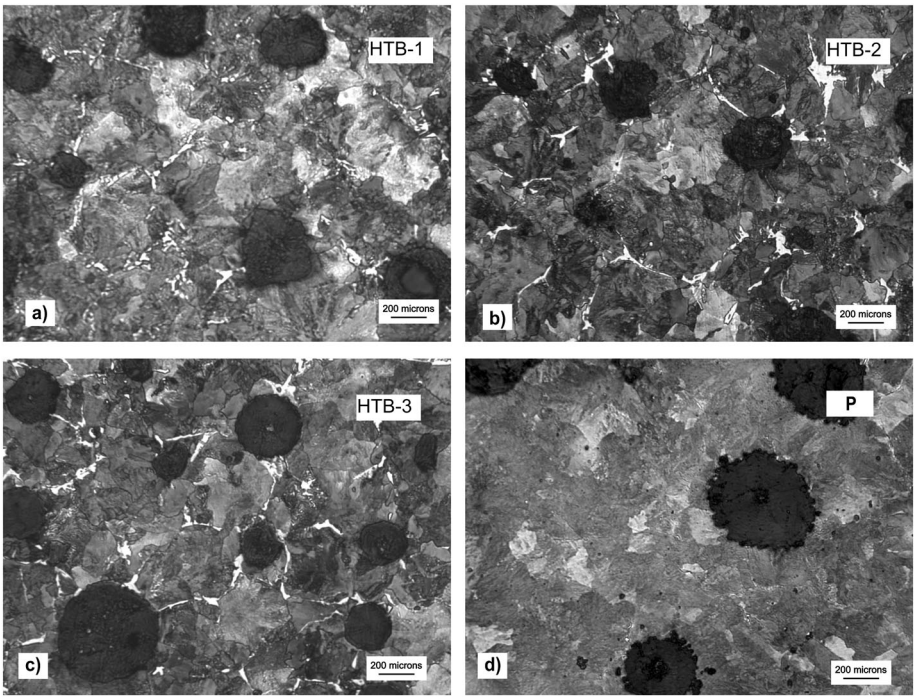


**Fig. 4** Micrographs of ferritic-pearlitic (HTB-1, HTB-2 and HTB-3) and fully pearlitic DI samples.

Significant enhancement of the mechanical properties with respect to a completely pearlitic matrix is reached, as shown by the results of the mechanical tests performed on these novel microstructures. The improvement is attributed to the fact that fine ferrite nets favour elongation until failure, leaving strength and hardness of the pearlite phase almost unaffected.

## Study of fracture surfaces

### *Dual-phase ADI samples*

The fracture surfaces of tensile test specimens were analysed by SEM. Figure 5 shows some of the fracture surfaces corresponding to the dual-phase ADI specimens obtained by HTA heat treatment together with those belonging to fully ferritic (F) and fully ausferritic (ADI) samples.

Figure 5a displays a surface with an irregular topography and large deformation of the ferritic matrix, which distinguishes ductile fracture. This mechanism characterises ferritic DI fracture under monotonic loading at room temperature.[12–14] As already covered and reported in the literature, the mechanisms of fracture under static uniaxial loading at room temperature characterising DI are nucleation, growth and coalescence of microvoids.[15,16] It should be considered that DI features voids or holes in its microstructure, as a result of the existence of nodular cavities and possible microvoids located in the last-to-freeze (LTF) zones, generated during solidification. These regions are considered weak areas within the metallic matrix, and typical casting defects such as inclusions, porosity and microshrinkage are present in these regions. Given these inherent flaws present, properties in monotonic tension loading should be governed by the growth and coalescence stages of these voids.

Because of the substantial plastic deformation experienced by the ferritic matrix, the spaces between nodules show a high degree of deformation in this fracture

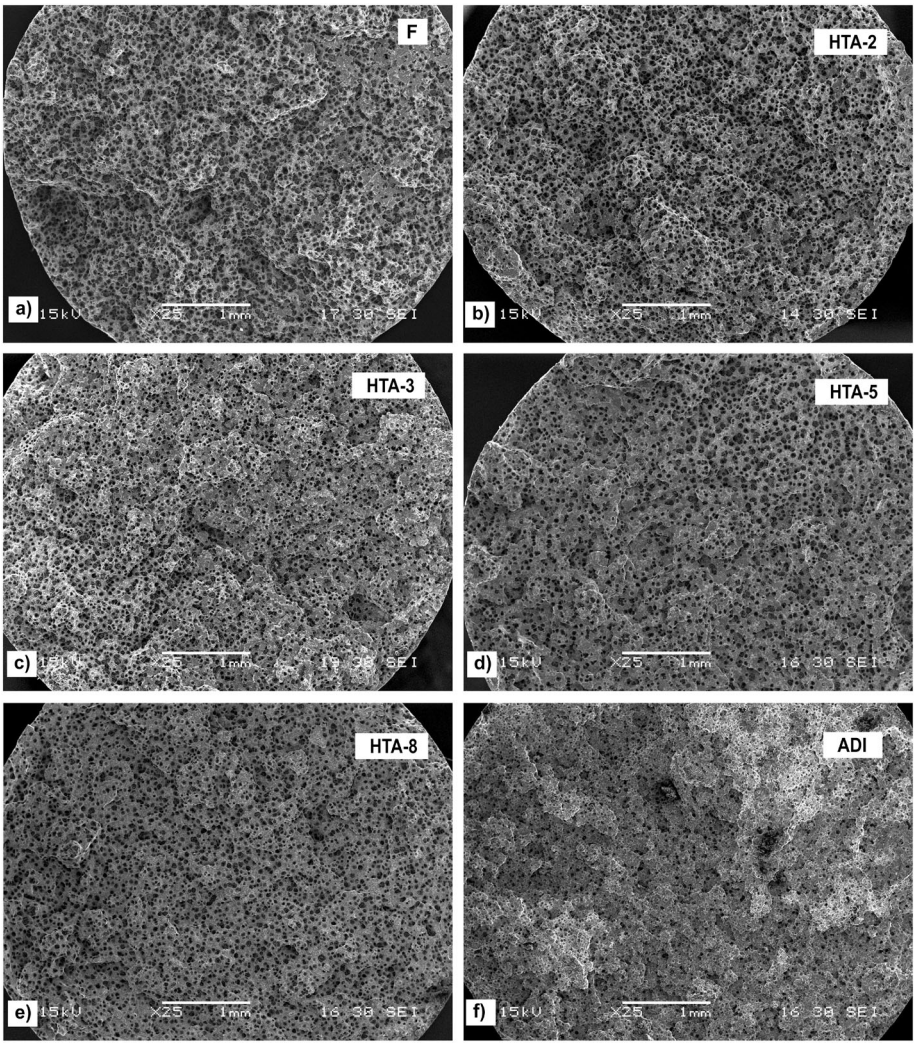


**Fig. 5** Fracture surfaces corresponding to samples: a) F, b-e) Dual Phase ADI, and f) ADI (Austempering temperature = 350 °C).

surface. The coalescence of voids represented by the graphite nodules interacting with the microvoids and other defects present in the LTF zones explains this behaviour. At the final stage of the coalescence, just before fragmentation, the high degree of deformation produces a sharp boundary or lip at internodular spaces.

Figure 6 depicts the fracture surface shown in Fig. 5a at higher magnification. The dimple pattern fracture and the high deformation around the cavities corresponding to graphite nodules can be seen, suggesting their growth before the final fracture event. This figure also displays the presence of an LTF zone, where different particles (possibly non-metallic oxides) cluster. On the other hand, the large deformation undergone by the matrix becomes evident.

Figure 5b shows the fracture surface of HTA-2 sample, containing 15% of ausferrite in the microstructure. The topography is similar to that found in the ferritic matrix (F sample), although at higher magnification (Fig. 7). However, the appearance of quasi-cleavage fractures can be found, typically in flat fracture surface zones, related to the presence of ausferrite located around LTF zones. Cleavage and ductile fractures coexist in this mechanism. Therefore, the internodular zones present dimple rupture combined with some quasi-cleavage sites, probably generated when the propagating crack travels through ausferritic and LTF zones.

This particular matrix (HTA-2 sample) is worth analysing, because this kind of microstructure has shown increase in tensile strength and yield stress in comparison with the ferritic matrix (F sample). With respect to fully ferritic DI, nodules and LTF zones are surrounded by ferrite, a phase with low strength and high strain properties when compared with other phases (pearlite, martensite or ausferrite). As a result, void (nodular cavities) or defect growth in LTF zones takes place at relatively low stress and large deformation. Then, fracture occurs in ductile mode, displaying a surface of irregular topography. The small amount of ausferrite in the matrix (less than 30%) is usually detected surrounding LTF zones (Figs 3b and 8), as evidenced in previous works by different authors.[4–8] This would lead to LTF zones encapsulation with a high resistance phase. As a result, microvoids growth in the LTF zones is delayed, leading to an increase in tensile properties.

Figure 5c shows the fracture surface of the HTA-3 specimen containing 60% of ausferrite in the matrix. The fracture surface exhibits a 'flatter' aspect, with decrease in the deformation of nodular cavities with respect to F and HTA-2 samples (micrographs 5a and 5b). The presence of higher amounts of ausferrite in the matrix generates a flat fracture surface, characteristic of quasi-cleavage fracture mechanics.[8,17,18] Figure 5d illustrates the fracture surface of the HTA-5 sample containing 80% ausferrite in its microstructure. The features of the fracture surface are similar to those noticed in the HTA-3 sample, with lesser plastic deformation zones evidently linked to the presence of free ferrite (Fig. 9). Tested samples with this structure revealed an

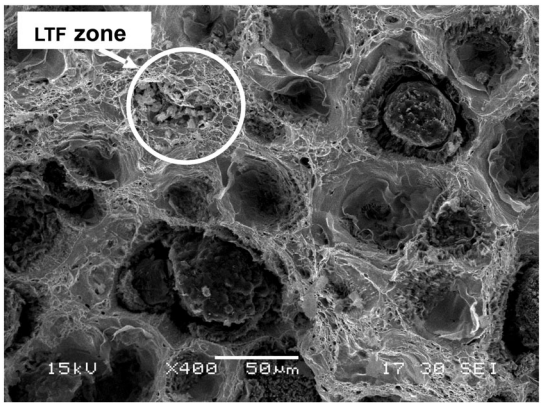


**Fig. 6** Detail of fracture surface of F sample (fully ferritic matrix).

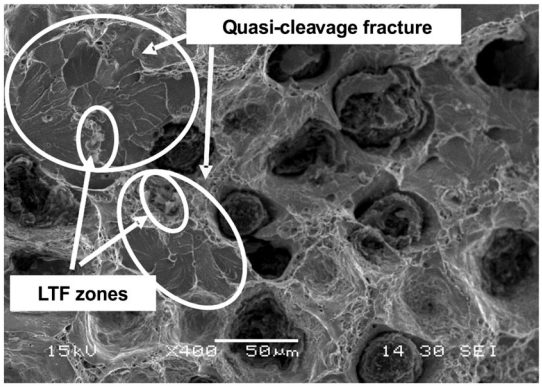


**Fig. 7** Detail of fracture surface of HTA-2 sample, containing 15% ausferrite in the microstructure.

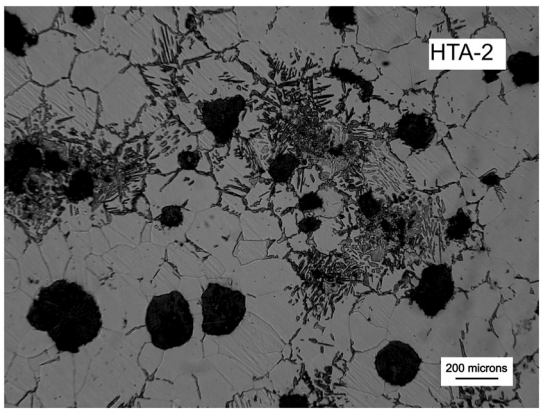


**Fig. 8** Micrographs of HTA-2 sample, containing 15% of ausferrite located preferentially surrounding LTF zones.

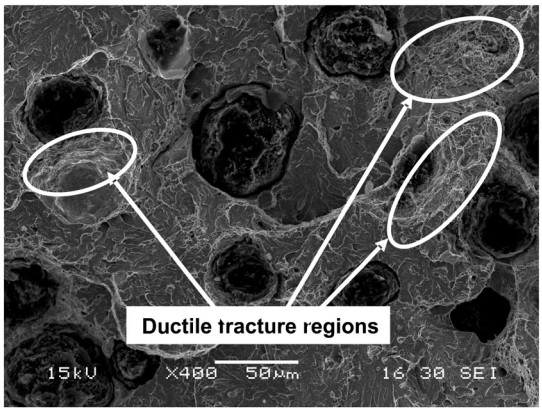


**Fig. 9** Detail of the fracture surface of HTA-5 sample, containing 80% ausferrite in its microstructure.

increase in tensile strength of about 40% (521–800 MPa) compared with F samples, with a small ductility loss (25–23%). This can be explained by the fact that LTF zones and nodular cavities are virtually surrounded by ausferrite in this microstructure (Fig. 9). This leads to an increase in the stress needed by these voids to grow and results in improved tensile strength, whereas ferrite plasticity allows it to maintain a high deformation capacity, typical of ferritic DI.

Figure 5e illustrates the fracture surface of the HTA-8 sample containing 5% ferrite and 95% ausferrite in its microstructure. The topography shows an even flatter aspect and slightly deformed nodular cavities, if compared with the fracture surfaces described earlier. Finally, the fully ausferritic microstructure keeps the trend described in the sequences analysed (Fig. 5f). This surface presents the flattest topography with the least deformed nodular cavities of all the fracture surfaces studied. The ADI sample exhibits the highest strength and lowest deformation. Ferrite presence allows greater growth of nodular cavities during the fracture process, which is reflected in greater deformation of these holes in the fracture surface (Fig. 5e versus Fig. 5f). This would justify the increase in the elongation until failure values yielded by the HTA-8 microstructure (16%) with respect to those encountered in ADI microstructures (10%) (Table 2). On the other hand, the remaining ausferrite keeps the tensile strength values of the ADI sample.

### *Ferritic–pearlitic samples*

Figure 10 illustrates the fracture surfaces corresponding to ferritic–pearlitic specimens and to a fully pearlitic (P) sample. The topography features a flat aspect and slightly or undeformed nodular cavities. Moreover, a dimple pattern in ferritic–pearlitic samples can be observed. This is more noticeable in HTB-1 to HTB-3 samples. Again, the presence of ferrite would justify the increase in the elongation until failure values yielded by the ferritic–pearlitic microstructure as compared with that found in fully pearlitic microstructures (Table 3).

Pearlite is a matrix with a limited plastic deformation capacity and predominantly exhibits brittle fracture with

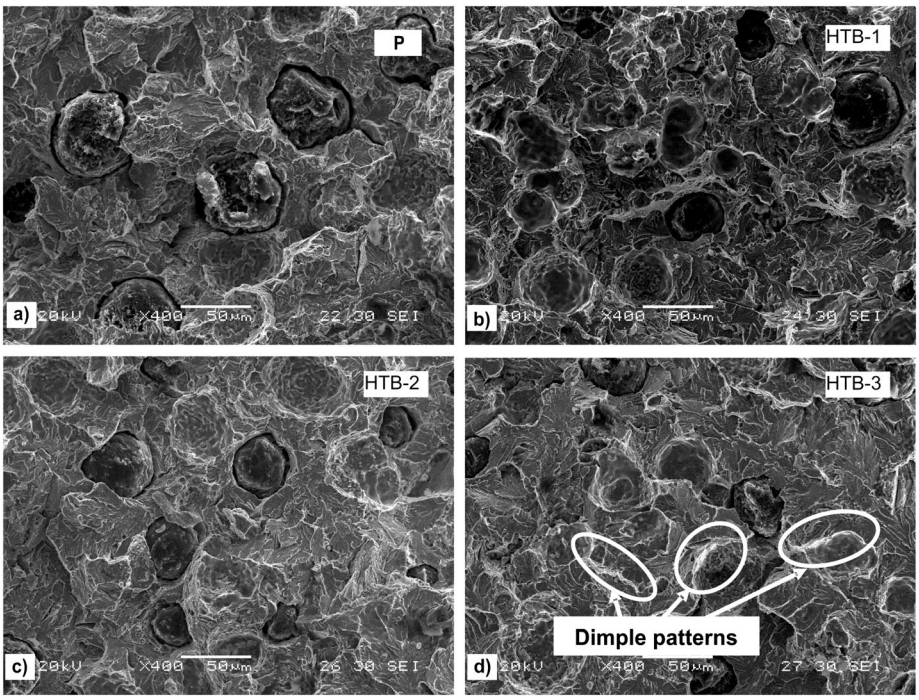


**Fig. 10** Fracture surfaces corresponding to samples: a) P, b-d) ferritic-pearlitic samples.

river patterns. It is evident that the fracture surface differs from that with ferritic or ausferritic microstructures, resulting in a flat surface with nodular cavities practically unstrained. The type of fracture consists in a crack propagating along well-defined low index crystallographic planes known as cleavage planes. Cleavage fractures are transgranular low energy fractures that mainly derive from the separation of atomic bonds at low index atomic planes. In view of the fact that cleavage always occurs along well-defined crystallographic planes within each grain, cleavage fractures change directions when they cross grain or sub-grain boundaries, graphite nodules, LTF imperfections and others, which explains the aforementioned river patterns observed.

### *Final considerations*

The observed operative mode of fracture at room temperature when slow load is applied to microstructures having high plasticity is the classic ductile tearing with the coalescence of microvoids. As a product of this mechanism, the fragmented matrix shows cup-like features of different sizes, which are governed by the size and distribution of the previous voids.

Cleavage fractures occurring commonly in high strength (low plasticity) microstructures tend to begin at the inclusions around the eutectic cell boundary (LTF) rather than at the graphite nodule–matrix interface. LTF zones are the starting point for the cleavage mechanism rather than the interface nodule–matrix. Figure 11 sketches a proposed model for both fracture models mentioned earlier.

In matrices with higher strength and toughness, the spherical discontinuities present in the material feature a lower deformation percentage, and hence defects, carbides and martensite (induced by strain transformation of retained austenite) present in the LTF zones play a key role in the fracture mechanism. This is the case of DI with an ausferritic matrix (ADI). The appearance of the fracture surface is quasi-cleavage, composed of zones with ductile fractures and facets of cleavage.

## CONCLUSIONS

1- To study the mechanical properties of dual-phase austempered ductile iron ('dual phase' ADI), this paper presents a fracture surface analysis of tensile samples. Several dual-phase ADI microstructures made up of different percentages of ausferrite and free ferrite were examined by SEM with this aim in mind. Samples with ferritic–pearlitic microstructures were analysed too.

2- The mechanisms of fracture characterising DI under static uniaxial loading at room temperature are nucleation, growth and coalescence of microvoids. The fracture surface of the fully ferritic DI presented an irregular topography with a dimple pattern and large deformation of the nodular cavities, characteristic of ductile fracture.

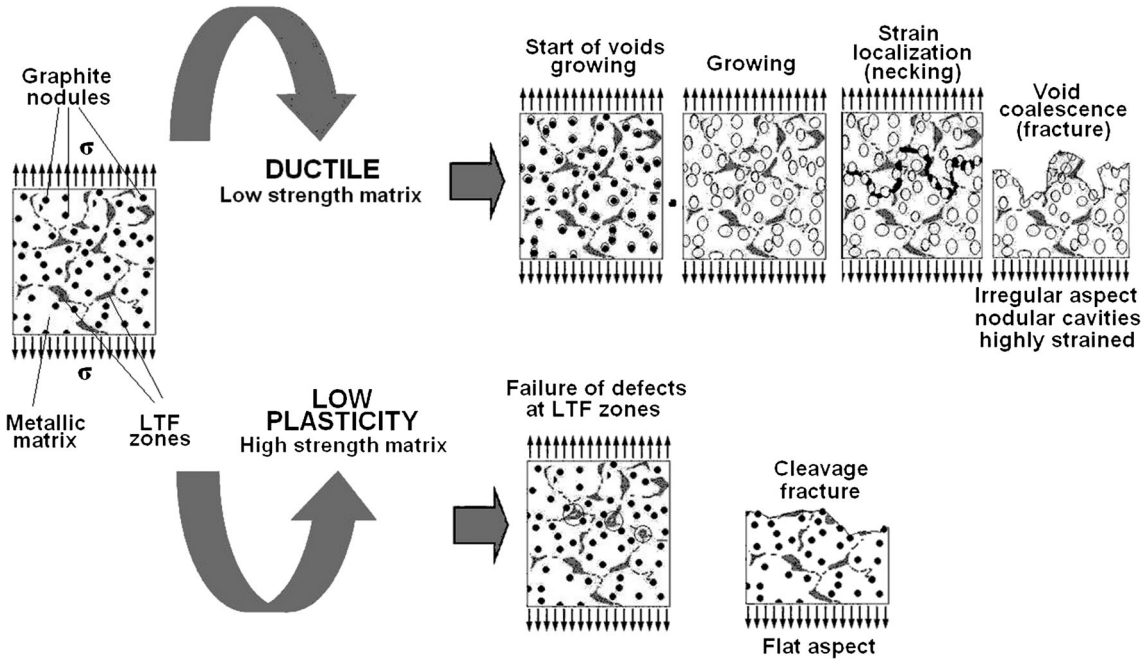


**Fig. 11** Proposed model for ductile and cleavage fracture modes with slow monotonic tension load.

3- Dual-phase ADI microstructures with small percentages of ausferrite in their matrix (less than 20%) showed an increase in mechanical properties with respect to fully ferritic matrices. These microstructures displayed regions of quasi-cleavage fractures around LTF zones, ascribed to the presence of ausferrite in those areas.

4- When the amount of ausferrite increased, so did tensile strength and yield stress, whereas elongation diminished slightly. Interesting combinations of strength and elongation were found, for example, the dual-phase microstructure composed of 20% ferrite and 80% ausferrite combined a tensile strength of 800 MPa with an elongation until failure of 23%. The presence of higher amounts of ausferrite resulted in a decrease in cavity nodules deformation and flatter fracture surface topography.

5- Compared with ADI samples, dual-phase microstructures containing 5% ferrite and 95% ausferrite maintained tensile strength and yield stress and had approximately 60% higher elongation until failure value. The presence of ferrite permitted greater growth of nodular cavities during the fracture process, which was reflected in greater deformation of these holes in the fracture surface, whereas the remaining ausferrite maintained the tensile strength values of the ADI sample.

6- By means of a thermal cycle called HTB, microstructures comprising pearlitic matrices containing a continuous and well-defined net of allotriomorphic ferrite, located at the grain boundaries of recrystallised austenite, were produced. The results of the mechanical tests performed on these microstructures revealed a significant enhancement of the mechanical properties with respect to completely pearlitic matrices. This is attributed to the fact that fine ferrite nets favour elongation until failure, leaving strength and hardness almost unaffected. The topographies of the fracture surfaces displayed a flat aspect and slightly or undeformed nodular cavities, as a result of the high amount of pearlite. A dimple pattern associated to ferritic regions could be observed.

## Acknowledgements

The financial support granted by CONICET, SECYT and the Universidad Nacional de Mar del Plata is gratefully acknowledged.

## REFERENCES

1 Aranzabal, J., Serramoglia, G. and Rousiere, D. (2002) Development of a new mixed (ferritic–ausferritic) ductile iron for automotive suspension parts. *Int. J. Cast Met. Res.* **16**, 185–190.
2 Wade, N. and Ueda, Y. (1981) Mechanical properties of ductile cast iron with duplex matrix. *Transactions ISII* **21**, 117–126.
3 Verdu, C., Adrien, J. and Reynaud, A. (2005) Contributions of dual phase heat treatments to fatigue properties of SG cast irons. *Int. J. Cast Met. Res.* **18**, 346–354.
4 Basso, A., Martinez, R. and Sikora, J. (2007) Influence of austenitising and austempering temperatures on microstructure and properties of dual phase ADI. *Mater. Sci. Technol.* **23**, 1321–1326.
5 Basso, A., Martinez, R. and Sikora, J. (2008) Influence of part size on dual-phase ADI microstructure and properties: comparison with fully ferritic and fully ausferritic matrices. *Mater. Sci. Technol.* **25**, 1271–1278.
6 Kilicli, V. and Erdogan, M. (2006) Tensile properties of partially austenitised and austempered ductile irons with dual matrix structures. *Mater. Sci. Technol.* **22**, 919–928.
7 Kilicli, V. and Erdogan, M. (2007) Effect of ausferrite volume fraction and morphology on tensile properties of partially austenitised and austempered ductile irons with dual matrix structures. *Int. J. Cast Met.* **20**, 202–214.
8 Kilicli, V. and Erdogan, M. (2010) The nature of the tensile fracture in austempered ductile iron with dual matrix microstructure. *J. Mater. Eng. Perform.* **19**, 142–149.
9 Mc Graw. (1968) *Quantitative Microscopy. Chapter 3: Measurement of Volume in Volume*. First edn. Hill Book Company, New York.
10 Basso, A., Martinez, R. and Sikora, J. (2011) Characteristics of the transformations occurring within the intercritical interval of ductile iron. *Key Eng. Mater.* **457**, 145–150.
11 Galarreta, I., Boeri, R. and Sikora, J. (1997) Free ferrite in pearlitic ductile iron. *Int. J. Cast Met. Res.* **9**, 353–358.
12 Celik, O., Ahlatci, H., Kayali, S. and Cimenoglu, H. (2005) High temperature abrasive wear behavior of an as-cast ductile iron. *Wear* **258**, 189–193.
13 Eldoky, L. and Voigt, R. (1985) Fracture of ferritic ductile iron. *AFS Trans.* **103**, 365–372.
14 Di Cocco, V., Iacoviello, F. and Cavallini, M. (2010) Damaging micromechanisms characterization of ferritic ductile cast iron. *Eng. Fract. Mech.* **77**, 2016–2023.
15 Voigt, R. and Eldoky, L. (1986) Fracture of ductile irons with dual matrix. *AFS Trans.* **94**, 645–656.
16 Martínez, R., Boeri, R. and Sikora, J. (2000) Mecanismos de fractura en fundiciones de grafito esferoidal austemperizada – ADI, Jornadas SAM 2000 - IV Latin-American Colloquium on Fracture and Fatigue, 615–622.
17 Masud, L., Martinez, R., Simison, S. and Boeri, R. (2003) Embrittlement of austempered ductile iron on contact with water—testing under applied potential. *J. Mater. Sci.* **38**, 2971–2977.
18 Martinez, R. (2010) Fracture surfaces and the associated failure mechanisms in ductile iron with different matrices and load bearing. *Eng. Fract. Mech.* **77**, 2749–2762.